Ab initio studies of ground and excited electronic states of MgAr, CdAr, and BeAr*

Jerry A. Boatz, **Keld Lars Bak***, **and Jack Simons**
Department of Chemistry, University of Utah, Salt Lake City, UT 84112, USA

Summary. The ground state ($X\ ^1\Sigma^+$) and several excited state ($A\ ^3\Pi$, $c\ ^3\Sigma^+$, $C\ ^1\Pi$, $D\ ^1\Sigma^+$, and $E\ ^3\Sigma^+$) potential energy surfaces for the diatomic molecules MgAr, CdAr, and BeAr have been computed using complete active space self-consistent field (CASSCF) wavefunctions and valence double- and triple-zeta quality basis sets augmented with polarization and diffuse functions. Pump-and-probe laser experiments have examined the quenching, of excited singlet states of metal-rare gas complexes such as CdXe to produce triplets that dissociate to ^3P_J metal atoms. This quenching, which is detected for CdXe but not for CdAr or MgAr, is thought to occur via a crossing or strong coupling of a repulsive triplet curve correlating to the underlying ^3P state of the metal, with an attractive singlet curve that correlates to the higher ^1P state of the metal. The present work indicates that the attractive $C\ ^1\Pi$ and repulsive $c\ ^3\Sigma^+$ curves of MgAr and CdAr *do not intersect* in the energetically accessible region of the $C\ ^1\Pi$ surface, unlike the corresponding curves for the CdXe diatom. These data are consistent with the absence of ^3P_J Cd atoms in the MgAr and CdAr experiments, respectively. However, an alternative quenching mechanism involving "vibronic" coupling between the $C\ ^1\Pi$ vibrational eigenstates and the continuum eigenstates of the underlying repulsive $^3\Sigma^+$ surface may be operative; this possibility is examined qualitatively and predicted to be unlikely for MgAr (due to small spin-orbit coupling) and CdAr (due to unfavorable vibronic factors). BeAr, which has yet to be probed experimentally, is predicted to be bound by 770 and 900 cm^{-1} in the $D\ ^1\Sigma^+$ state (which has metal $2s2p$ character) and the $E\ ^3\Sigma^+$ state (which has Rydberg metal $2s3s$ character), respectively, and to display interesting potential curve intersections.

Key words: MgAr – CdAr – BeAr – Ground states – Excited states – CASSCF

---

1. Introduction

1.1. The ground and low-energy excited triplet and singlet states of alkaline earth + noble gas species

The alkaline earth-rare gas and other similar van der Waals diatomic systems have been the focus of several recent experimental [1–7] and theoretical [8–14] studies. Of primary interest in these works is the characterization of both the weakly-bound van der Waals ground-state complex [3, 6–10, 14] and low-lying singlet and triplet excited state [1–7, 10–13] potential energy surfaces of these molecules.

Experimental studies of MgAr [3] and CdAr [6] (as well as other similar systems [2b, 2d]) indicate that the binding on the ground-state potential energy surface, which connect to an $ns^2\,^1S$ ground-state atom and the nobel gas, is primarily due to a weak van der Waals interaction and produces large equilibrium internuclear distances ($r_e = 4.49$ and 4.33 Å, respectively [3, 6]). In contrast, the $C\,^1\Pi$ and $A\,^3\Pi$ states of MgAr, which correlate, respectively, to the $3s3p\,^1P$ and ^3P states of Mg + Ar, are bound by over $300\,\mathrm{cm}^{-1}$ and have considerably smaller r_e's (3.27 and 3.63 Å, respectively [4]).

Furthermore, the $E\,^3\Sigma^+$ Rydberg state (e.g., having appreciable $(3s)^1(4s)^1$ character for MgAr) is bound by over $1100\,\mathrm{cm}^{-1}$ (see Fig. 1a.) The presence of minima on these potential energy surfaces can be understood in terms of an ion-induced dipole model in which the rare-gas atom is attracted to a partially shielded Mg^+ ion core. In the Π states, the Π orientation of the singly-occupied p orbital on Mg allows for a closer approach of the rare-gas atom than when the p orbital is in the Σ orientation [3]. Similarly, in the Rydberg state, provided the approaching rare-gas atom penetrates the spatially diffuse Rydberg orbital (which induces a slight initial repulsion at long internuclear distances), it will again be attracted to a partially shielded Mg^+ ion core.

1.2. Notation for state labels

For the MgAr species, potential energy curves for all of the states mentioned above are shown. The notation used for labelling these states is taken from the work of Breckenridge et al. It is probably not spectroscopically appropriate to use this same labelling for all three of the species (CdAr, MgAr, and BeAr) studied here because the spin-orbit interaction is small in Be and quite large in Cd. Nevertheless, in order to better show the *similarities* and differences among the potential curves of the three species, we have chosen to adopt one convention (used in [3] for MgAr) and to use this to label the states of BeAr, MgAr, and CdAr.

1.3. The laser pump-probe experiments and quenching

In the laser pump-probe experiments [2, 3, 6, 7], $X\,^1\Sigma^+$ ground-state metal-rare-gas (i.e., Mg · RG) molecules are excited to the $^1\Pi$ surface and subsequent appearance of ^3P_J atoms is monitored. Production of triple M is thought to occur via crossing of the repulsive $c\,^3\Sigma^+$ state and the initially populated $C\,^1\Pi$ state. That is, the lower-lying repulsive $c\,^3\Sigma^+$ state (which correlates at infinite

separation with ^3P M + ^1S Ar) intersects an energetically accessible region of the bound $C\,^1\Pi$ state.

This supposition is primarily based upon experimental studies of the CdXe diatom, where production of the $C\,^1\Pi$ state leads to efficient production of ^3P_J Cd atoms via a spin-orbit coupling between the bound $C\,^1\Pi$ state and the dissociative $c\,^3\Sigma^+$ state [7]. Indeed, virtually *no* fluorescence from the $C\,^1\Pi$ state is observed at all in CdXe.

However, in analogous experiments on CdAr [6], just the opposite occurs; namely, fluorescence of the $C\,^1\Pi$ state is prevalent, with no detectable formation of ^3P_J Cd atoms. This is rather puzzling, since it seems reasonable to expect the potential curves and the strength of the spin-orbit coupling of CdXe and CdAr to be quite similar. Likewise, no production of ^3P_J Mg atoms is observed after the formation of $C\,^1\Pi$ MgAr [3], although this is less surprising since the spin-orbit coupling in Mg is considerably less than that in Cd.

1.4. Past theoretical work

Prior theoretical studies of MgAr include the all-electron fourth-order Møller–Plesset calculations [9] on the ground state and the perturbative calculations [10] of the dispersion energies of the lowest singlet and triplet Σ, Π, and Δ excited states (as well as the ground state). Similar calculations have been performed for CdAr [12] and related systems [12, 13]. Apparently the only prior calculation on BeAr has been a rather approximate calculation of its ground-state potential energy surface, at the SCF level [14].

The purpose of the present work is to investigate the validity of the physical pictures introduced above and to identify regions of surface intersections and/or avoided crossings for the molecules MgAr, CdAr, and BeAr. To this end, *qualitatively* correct potential energy surfaces are calculated for the electronic states of interest.

2. Computational methods

2.1. Treatment of electron correlation – van der Waals interactions are not included

In order to obtain a balanced description of all electronic states considered here, complete active space self-consistent field (CASSCF) wavefunctions were employed. The active space consisted of the two $3s$ electrons of Mg, distributed in all possible ways among the $3s$, $3p$, $4s$, and $4p$ Mg orbitals. This space generates 16, 8, 8, and 8 configuration state functions (CSFs) of $^1\Sigma^+$, $^3\Sigma^+$, $^1\Pi$, and $^3\Pi$ symmetry, respectively.

It should be noted that not including any of the electrons and orbitals on Ar in the active space excludes from the calculation those CSFs required to describe dispersion interactions, which are necessary for quantitatively accurate calculations of weak intermolecular interactions. Hence, these calculations cannot predict the presence of shallow wells in the $X\,^1\Sigma^+$, $C\,^1\Pi$, $A\,^3\Pi$, and $E\,^3\Sigma^+$ states; that is, our calculations *do not include any van der Waals* interactions.

However, the primary objective of this study is not a quantitatively accurate description of well depths and bond lengths. These data are much more

accurately known from interpretations of the experimental data; they are discussed later in Sect. 3 where our results are presented. In this paper, we are seeking a qualitatively correct picture of the individual potential energy surfaces which will allow us to identify, among other features, probable regions of intersections and/or avoided crossings between electronic states.

2.2. Atomic orbital basis sets and superposition error corrections

The basis sets used in this study are summarized in Table 1. For all three molecules, the effective core potential (ECP) and the companion valence double-zeta basis set of Stevens, Basch, and Krauss [15] were used for Ar. The valence basis was augmented with a single set of diffuse s and p functions as well as two sets of five d-type polarization functions. (See Table 1 for the values of the exponents used.) In order to test the validity of using an effective core potential on Ar, the calculations of all the potential energy curves of BeAr were repeated using an all-electron treatment of Ar. Virtually identical potential energy curves are obtained for all of the electronic states. For the all-electron calculations, the Ar basis consisted of the McLean–Chandler ($12s9p/6s5p$) set [16] plus the same set of diffuse and polarization functions used in the ECP computations.

For each of the metal atoms considered in this work, the basis set used is constructed in a similar manner. Starting with a basis set which is at least of valence double-zeta quality, a single set of five d-type polarization functions are added. Next, in order to have a basis set which is sufficiently flexible to describe the triplet (ns) ($[n+1]s$) Rydberg states (i.e., $E\,^3\Sigma^+$), two sets of diffuse s and p functions are added (see Table 1 for the exponents). An exception is made for cadmium, for which only a single set of diffuse s and p functions were added. For magnesium, the McLean–Chandler ($12s9p/6s5p$) basis set [16] is used. The 6-311G basis set of Pople et al. [17] is used for beryllium. The ECP of Hay and Wadt [18] and the associated double-zeta valence basis set is used for cadmium. The MESSKIT [19] suite of computer programs was used in performing all energy calculations. All calculated potential energy curves were corrected for

Table 1. Summary of basis sets and effective core potentials

	Ar	Ar[d]	Mg	Cd	Be
ECP[a]	SBK	None	None	HW	None
Basis[b]	SBK DZ	MC	MC	HW DZ	6-311G[c]
α_s	0.027	0.027	0.0209, 0.00825	0.02176	0.0285, 0.01125
α_p	0.021	0.021	0.0152, 0.0060	0.0162	0.0171, 0.00675
α_d	1.70, 0.425	1.70, 0.425	0.175	None	0.400

[a] "SBK" ("HW") denotes the ECP from [15] (18)
[b] "SBK DZ" ("HW DZ") denotes the double-zeta valence basis defined in [15] (18). "MC" denotes the McLean–Chandler ($12s9p/6s5p$) basis from [16]
[c] See [17]
[d] Used only in the BeAr all-electron calculations

basis set superposition error using the counterpoise method of Boys and Bernardi [20].

3. Results and discussion

3.1. Atomic state energies

Let us first recall that we employ the MgAr state notation of [3] for CdAr, MgAr, and BeAr to maintain consistency throughout and to make comparisons more straightforward. In order to compare our calculations with experiment, the atomic energies of the metal atoms for states that correlate to the $X\,^1\Sigma^+$, $A\,^3\Pi$, $c\,^3\Sigma^+$, $C\,^1\Pi$, $D\,^1\Sigma^+$, and $E\,^3\Sigma^+$ molecular states of the $M \cdot RG$ complexes were calculated, using the same active space and basis sets as outlined in the previous section. The results are summarized in Table 2. With the exception of the Be $^1S \rightarrow {}^1P$ transition energy (which is about 0.9 eV too high), all calculated transition energies agree to within approximately 0.5 eV of the experimental values.

3.2. Diatomic potential curves

For ease of chemical interpretation, Table 3 summarizes the relationship between the spectroscopic notation for each electronic state and the dominant electron configuration, in terms of the orbitals on the metal atom.

**Table 2.** Calculated and experimental atomic excitation energies[a]

Atom	$^1S \rightarrow {}^3P$	$^1S \rightarrow {}^1P$	$^1S \rightarrow {}^3S$
Mg	2.71	4.78	4.98
	(2.69)	(4.34)	(5.12)
Cd	3.38	5.51	5.85
	(3.73)	(5.42)	(6.37)
Be	3.08	6.20	6.37
	(2.73)	(5.29)	(6.46)

[a] In eV. Experimental values (taken from Moore, C. E. "Atomic Energy Levels", Vols. 1 and 3, Nat. Stand. Ref. Data. Ser., NBS, 1971) are given in parentheses

Table 3. Dominant electron configuration for each electronic state

Electronic state	Configuration
$X\,^1\Sigma^+$	$(ns)^2$
$A\,^3\Pi$, $C\,^1\Pi$	$(ns)^1(np_\pi)^1$
$c\,^3\Sigma^+$, $D\,^1\Sigma^+$	$(ns)^1(np_\sigma)^1$
$E\,^3\Sigma^+$	$(ns)^1([n+1]s)^1$

Our calculated potential energy curves for MgAr, CdAr, and BeAr are shown in Figs. 1a, 1b, and 1c, respectively. No local minima are observed in any of the MgAr and CdAr curves because, as mentioned earlier, our calculations intentionally exclude the van der Waals interaction configurations. This is done because to include such configurations would render the calculations prohibitive, and because we have no hope of computing these dispersion energies accurately
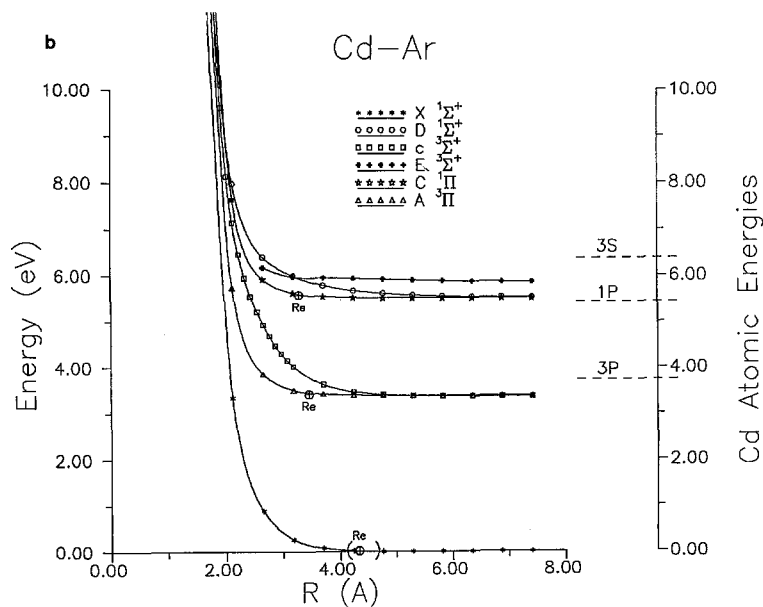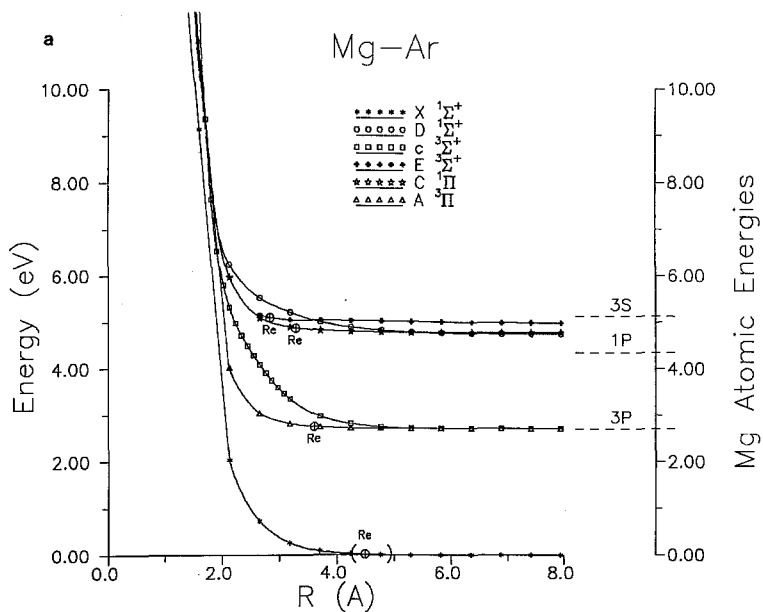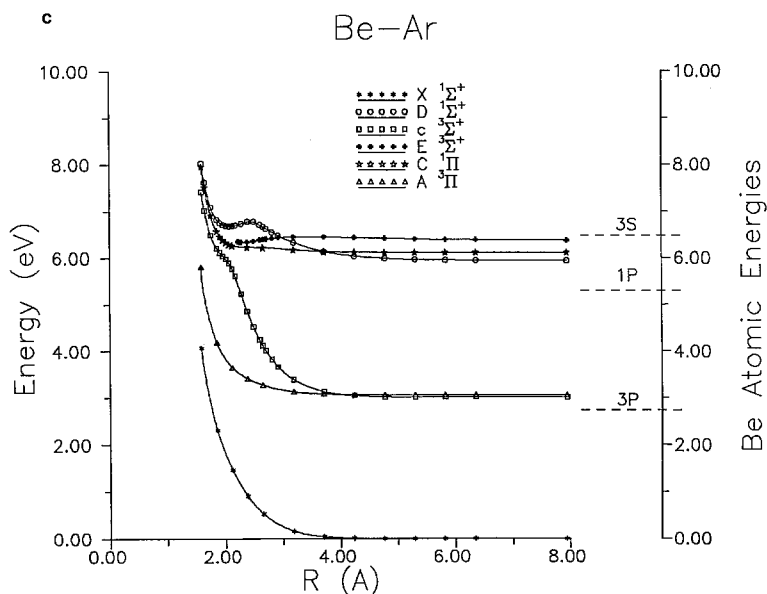
Fig. 1. a Calculated potential energy surfaces of MgAr, with the experimentally determined equilibrium bond lengths denoted "Re" and the ground-state $v = 0$ turning points shown by ( ). **b** Calculated potential energy surfaces of CdAr, with the experimentally determined equilibrium bond lengths denoted "Re" and the ground-state $v = 0$ turning points shown by ( ). **c** Calculated potential energy surfaces of BeAr

enough to be of use. Let us now examine each of the metal + noble gas species in further detail.

3.2.1. MgAr. Figure 1a shows that the $X\,^1\Sigma^+$ potential remains "flat" until the internuclear distance R decreases to about 4 Å, after which it rises quite sharply. From [3] we know that this state has a minimum near 4.5 Å with a depth of $D_e = 83\ \mathrm{cm}^{-1}$.

The $A\,^3\Pi$ and $c\,^3\Sigma^+$ states, which are degenerate at $R = \infty$, remain nearly flat until R decreases to about 5 Å. At this point, the $c\,^3\Sigma^+$ surface begins to rise in energy while the $A\,^3\Pi$ state remains level until R reduces to near 4 Å. The $^3\Pi$ state is thought [3] to possess a minimum near 3.6 Å with a depth of $D_e = 300\ \mathrm{cm}^{-1}$.

Similar behavior is observed for the $C\,^1\Pi$ and $D\,^1\Sigma^+$ states (which are also degenerate at infinite separation, in the absence of spin-orbit coupling), although the $C\,^1\Pi$ state is less strongly repulsive than its triplet counterpart. The latter $^1\Pi$ state is thought [3] to have a minimum near 3.3 Å with a depth of $D_e = 368\ \mathrm{cm}^{-1}$. Finally, the $E\,^3\Sigma^+$ Rydberg state remains level until R decreases to 3 Å, and thus behaves similarly to the Π states.

These above behaviors of the valence and Rydberg states of MgAr are consistent with a fractional charge-induced dipole model [3], which states that the Π orientation of the singly-occupied p orbital on Mg allows for a closer approach of the argon atom than does the Σ orientation.

Of particular interest in Fig. 1a are the relative locations of the $C\,^1\Pi$ and $c\,^3\Sigma^+$ curves. Based on experimental studies on CdXe [7], which has a well

2500 cm^{-1} deep on its $^1\Pi$ surface, it had been anticipated that these two curves intersect in an energetically accessible region of the $C\,^1\Pi$ surface; i.e., at an energy below the asymptotic limit of ^1P Mg + ^1S Ar. Inspection of Fig. 1a shows that these curves intersect well above this limit. Even by adding the 363 cm^{-1} deep van der Waals- term to our $C\,^1\Pi$ potential, intersection does not occur below the ^1P Mg + ^1S Ar asymptote.

In Fig. 2a, the $C\,^1\Pi$ and $c\,^3\Sigma^+$ curves have been shifted so that the asymptotic ^1P Mg + ^1S Ar and ^3P Mg + ^1S Ar energies match the experimental values. Even then, and even if the above 363 cm^{-1} of van der Waals attraction is added, the intersection of these two curves still occurs far above the asymptotic ^1P Mg + ^1S Ar limit.

While it is possible that the level of calculation here is inadequate to correctly describe the behavior of the $C\,^1\Pi$ and $c\,^3\Sigma^+$ states for small internuclear distances, it is also possible that a mechanism other than curve crossing exists whereby a spin-orbit assisted transition between these two states can take place. Although it seems unlikely that these curves actually intersect at an energy below that of ^1P Mg + ^1S Ar, it seems quite probable that these curves will closely approach each other for energies near this energy limit. This in turn could allow for a large overlap between the vibrational eigenstates of the bound $C\,^1\Pi$ state with the isoenergetic continuum eigenstates of the repulsive $c\,^3\Sigma^+$ state. This possibility, which requires that spin-orbit coupling also be operative, will later be explored in greater detail (vide infra).

3.2.2. CdAr. Our computed potential energy curves of CdAr are found in Fig. 1b and are quite similar to those of MgAr (see Fig. 1a). As in MgAr, the ground-state potential starts to rise in the vicinity of $R = 4$ Å; this potential is known [6] to have a minimum at 4.3 Å that is $D_e = 106 \text{ cm}^{-1}$ deep.
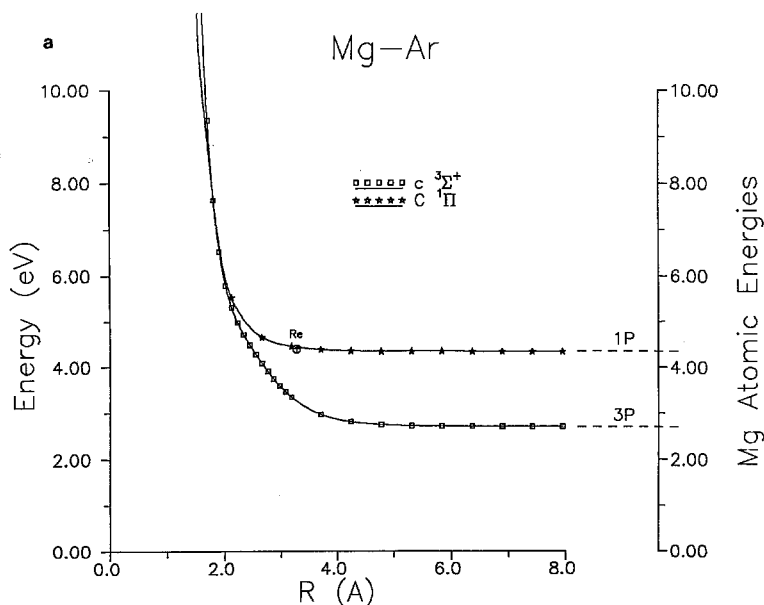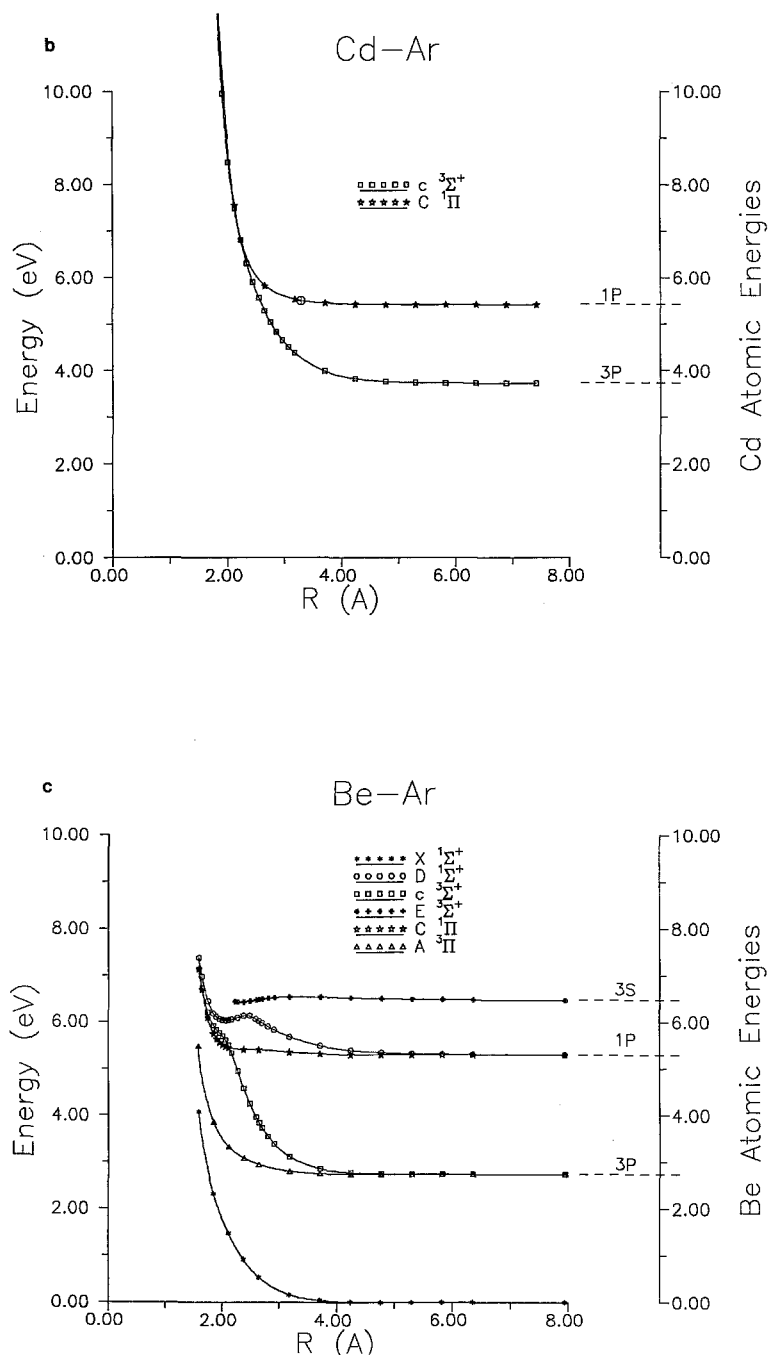
Fig. 2. a Calculated $C\ ^1\Pi$ and $c\ ^3\Sigma^+$ potential energy surfaces of MgAr, shifted to asymptotically match the experimental energies of ^1P and ^3P Mg, respectively. **b** Calculated $C\ ^1\Pi$ and $c\ ^3\Sigma^+$ potential energy surfaces of CdAr, shifted to asymptotically match the experimental energies of ^1P and ^3P Cd, respectively. **c** Calculated potential energy surfaces of BeAr, shifted to asymptotically match the experimental energies of ^1P, ^3P, and ^3S Be

Both the $c\,^3\Sigma^+$ and $D\,^1\Sigma^+$ curves become repulsive at a slightly larger internuclear distance (near $R = 5$ Å) relative to MgAr. Inspection of Fig. 1b shows that the $c\,^3\Sigma^+$ and $C\,^1\Pi$ curves intersect at an energy well above the ^1P Cd $+\,^1S$ Ar limit. This is still true even after (i) these curves have been shifted so that the asymptotic energies match those of experiment (see Fig. 2b) and (ii) the $^1\Pi$ curve is allowed to adopt its 544 cm^{-1} deep van der Waals well [6] with a minimum near 3.3 Å.

Since the $c\,^3\Sigma^+$ and $C\,^1\Pi$ states seem likely not to intersect at an energy below ^1P Cd $+\,^1S$ Ar, the same vibronic interaction mechanism outlined above may again be the primary means of a transition between these two curves (vide infra). In this Cd case, the presence of stronger spin-orbit coupling will make this possibility even more likely.

3.2.3. BeAr. Figure 1c shows our calculated potential energy curves for BeAr. Here, there are no experimental data from which to obtain the equilibrium distances for the $X\,^1\Sigma^+$ or the $C\,^1\Pi$ states. However, it is virtually certain that these states will not possess minima that are any deeper than those found for MgAr (83 cm^{-1} and 368 cm^{-1}, respectively).

These BeAr surfaces exhibit the same general characteristics as those for MgAr and CdAr; namely, that the $c\,^3\Sigma^+$ and $D\,^1\Sigma^+$ curves become repulsive at longer R than do their Π counterparts and that an intersection between the $c\,^3\Sigma^+$ and $C\,^1\Pi$ curves at an energy below ^1P Be $+\,^1S$ Ar seems improbable.

However, unlike MgAr and CdAr, the calculated potential energy curves for BeAr show the presence of local minima in the $D\,^1\Sigma^+$ and $E\,^3\Sigma^+$ curves, with well depths of approximately 770 and 900 cm^{-1}, respectively. The former apparently is caused by an avoided crossing with a higher state of $^1\Sigma^+$ symmetry (not shown in Fig. 1c). The presence of a well on the $E\,^3\Sigma^+$ Rydberg surface is consistent with the fractional charge-induced dipole model as discussed in the Introduction. The "shoulder" on the repulsive limb of the $c\,^3\Sigma^+$ curve is apparently the result of an avoided crossing with the higher-lying $E\,^3\Sigma^+$ state. Note that in the region of this avoided crossing, the $c\,^3\Sigma^+$ state is diverted away from the $C\,^1\Pi$ curve. Consequently, if the latter two curves intersect, the point of intersection will occur at a smaller internuclear distance (and hence at a higher energy) than if the avoided crossing was absent.

As seen in Fig. 1c, the calculated $c\,^3\Sigma^+$ and $C\,^1\Pi$ curves of BeAr do not intersect below the ^1P Be $+\,^1S$ Ar energy. However, when these two curves are shifted to match the corresponding experimental asymptotic energies, their intersection occurs at an energy near the asymptotic limit (see Fig. 2c.) This result is in contrast to the analogous curves of MgAr and CdAr and suggests that, in the case of BeAr, predissociation to the $c\,^3\Sigma^+$ state from the $C\,^1\Pi$ surface may indeed take place via an actual curve crossing.

In Fig. 2c, *all* of the calculated potential energy curves of BeAr have been shifted so that their asymptotic energies match the corresponding experimental atomic energies of the Be atom. We believe that this gives a reasonably accurate picture of the ground and low-lying excited states of BeAr, and so the potential energy surfaces in Fig. 2c will form the basis of our discussion on the experimental implications of the wells on the $D\,^1\Sigma^+$ surfaces.

The presence of these wells is intriguing and suggests that these excited states of BeAr may be detectable in laser pump-probe experiments similar to those performed on MgAr [3, 4] and CdAr [5, 6]. In particular, if a metastable triplet BeAr complex on the (presumably bound) $A\,^3\Pi$ surface can be prepared in a

supersonic jet expansion (as is done for MgAr [4]), then laser excitation to the bound $E\,^3\Sigma^+$ Rydberg state should be possible. Furthermore, once triplet Rydberg BeAr has been prepared, several routes may then be taken to other states. Since the $c\,^3\Sigma^+$ and $E\,^3\Sigma^+$ states undergo an avoided crossing in the vicinity of the $E\,^3\Sigma^+$ minimum, a radiationless transition back to the $c\,^3\Sigma^+$ surface is possible. Note, however, that the degree to which these two states avoid each other is probably overemphasized in Fig. 2c. This is because the energy spacing of the corresponding *unshifted* curves in Fig. 1c (from which the curves in Fig. 2c are obtained) is somewhat smaller than indicated by the experimental Be atomic excitation energies.

Because the spin-orbit coupling is small for beryllium, a spin-forbidden transition from the $E\,^3\Sigma^+$ Rydberg state of BeAr to the underlying $D\,^1\Sigma^+$ state is unlikely to occur to a significant extent. However, such a transition could allow for the characterization of both the short-range attractive and long-range repulsive regions of the $D\,^1\Sigma^+$ surface.

3.3. Vibronic coupling

3.3.1. Both spin-orbit and angular non-adiabatic coupling must be brought into play. Although the $c\,^3\Sigma^+$ and $C\,^1\Pi$ curves of MgAr and CdAr apparently do not intersect at an energy below the ^1P Mg + ^1S Ar and ^1P Cd + ^1S Ar asymptotic limits, respectively, there still may exist other means by which these two potential energy surfaces can interact. Since these two curves are in close proximity at small internuclear distances, a possible mechanism is for a non-adiabatic coupling (of an angular type, i.e. involving $\partial/\partial\theta$ or $\partial/\partial\phi$ because a Σ and Π state are to interact) between the bound vibrational eigenstates of the $C\,^1\Pi$ state and the continuum eigenstates of the unbound $c\,^3\Sigma^+$ state. Of course, for such couplings to be operative significant spin-orbit interaction must *also* be present; this is more likely for CdAr than for MgAr.

The radial matrix elements arising in this non-adiabatic coupling are illustrated in Fig. 3, which shows a vibrational eigenfunction of a Morse potential
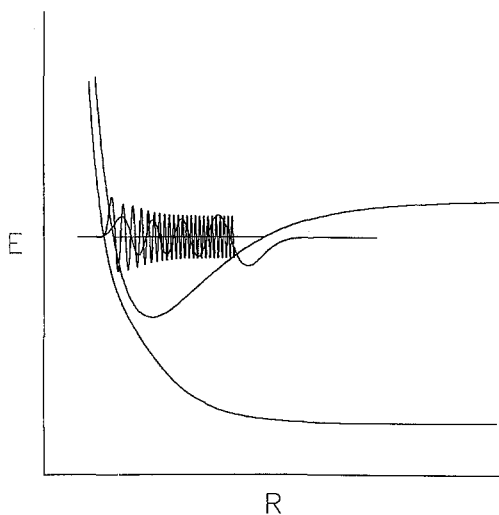
Fig. 3. "Vibronic" coupling between a vibrational eigenstate of a bound $^1\Pi$ state and the isoenergetic continuum eigenstate of an underlying dissociative $^3\Sigma^+$ state
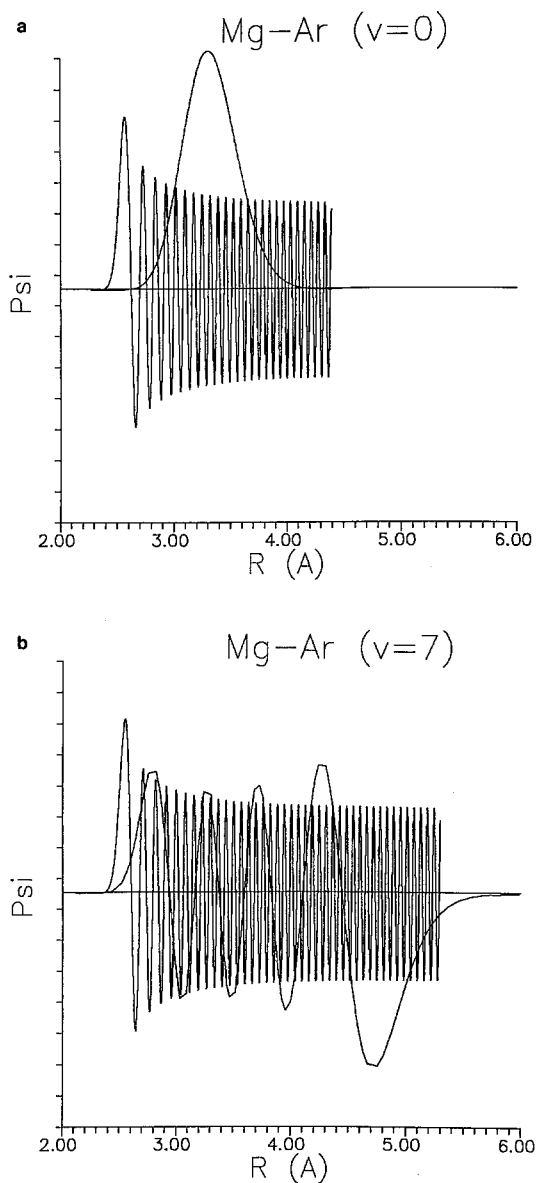
[21] and the isoenergetic continuum eigenfunction of the underlying repulsive triplet curve superimposed on their respective potential energy surfaces. The net overlap of these two eigenfunctions serves as an indication of the likelihood of a connecting vibronic interaction. Since the continuum eigenstate oscillates much more rapidly than does the Morse potential eigenstate, the overlap of these two functions is expected to be virtually zero except in the region of the repulsive "wall" where the two potential energy curves are in close proximity. In this region, the rate of oscillation of the continuum eigenfunction is reduced, which may allow for a nonzero overlap with the innermost "envelope" of the Morse potential eigenfunction.

3.3.2. Model calculations. In order to investigate the likelihood for such vibronic couplings in MgAr and CdAr, the $C\,^1\Pi$ states of these diatomics were modelled using Morse potentials, with the Morse parameters determined from fits to experimental r_e and D_e data referenced earlier [3, 6]. Our calculated triplet curves in Figs. 2a and 2b were used to represent the underlying $c\,^3\Sigma^+$ states. Then, for each experimentally observed vibrational level of the bound $C\,^1\Pi$ state, the corresponding Morse vibrational eigenfunction was computed. At the corresponding energy on the underlying $c\,^3\Sigma^+$ state, the continuum nuclear wavefunction was then computed. (Since the continuum eigenfunctions of MgAr and CdAr do not approach zero in the limit of large internuclear distances, they were "box-normalized" using an arbitrary length L which extended well beyond the outer envelopes of all of the Morse potential eigenfunctions calculated here.) Finally, the overlap was computed via numerical integration of the product of these two nuclear wavefunctions.

Obviously, because we do not have highly accurate representations of either the underlying $^3\Sigma$ curve or the weakly bound $^1\Pi$ curve, the results of these model calculations must be viewed as indicative of what *might* happen. Moreover, because we do not compute the *electronic* part of the non-adiabatic coupling matrix elements (the overall matrix element is a product of this electronic component and the vibrational component that we calculate), we are not able to evaluate the *absolute* rates of transitions. Nevertheless, we view it as valuable to show how the rates of coupling between various vibrational levels of the weakly bound $^1\Pi$ state and the underlying repulsive $^3\Sigma$ state *might* be expected to vary with vibrational quantum number v. Our calculated *relative* rates will be of use if the spin-orbit and electronic non-adiabatic coupling matrix elements vary less strongly with internuclear distance than does the vibrational overlap factors considered here.

3.3.3. MgAr. In MgAr, there are eight ($v = 0-7$) vibrational levels observed in the $C\,^1\Pi$ state [3]. Figures 4a and 4b show plots of the $v = 0$ and $v = 7$ vibrational eigenfunctions, respectively, of the $C\,^1\Pi$ state of MgAr superimposed with the corresponding *isoenergetic* continuum eigenfunctions of the underlying unbound $c\,^3\Sigma^+$ state. Of particular importance in these plots is the relative position of the innermost lobe of the Morse eigenfunction and the continuum eigenfunction, since the total overlap is determined primarily by the degree of overlap of these two envelopes.

For the $v = 0$ level of $C\,^1\Pi$ MgAr (Fig. 4a), the innermost envelope of the continuum eigenfunction occurs well within that of the Morse eigenfunction. Therefore, a small overlap is anticipated for this vibrational level. However, for $v = 7$ (Fig. 4b), one observes a significant non-zero overlap of the respective innermost envelopes and therefore a relatively large total overlap is expected.

a

Mg−Ar (v=0)

b

Mg−Ar (v=7)

Fig. 4. **a** Morse potential vibrational eigenfunction for the $v = 0$ vibrational level of $C\ {}^1\Pi$ MgAr and the isoenergetic continuum eigenfunction of the underlying $c\ {}^3\Sigma^+$ state. **b** Morese potential vibrational eigenfunction for the $v = 7$ vibrational level of $C\ {}^1\Pi$ MgAr and the isoenergetic continuum eigenfunction of the underlying $c\ {}^3\Sigma^+$ state

The results of the numerical integrations of the Morse potential eigenfunctions with the corresponding continuum eigenfunctions for all eight vibrational levels of MgAr are summarized in Table 4. There are two sets of values listed in Table 4. One set consists of the actual overlap magnitudes and the other set is the percentages of the maximum possible overlaps.

The latter values are defined as the overlaps which occur when the $c\ {}^3\Sigma^+$ state intersects the $C\ {}^1\Pi$ state *at the energy of the particular $C\ {}^1\Pi$ vibrational level*. The differences between these maxima and the observed overlaps are

Table 4. Values of nuclear wavefunction overlap integrals of MgAr[a]

Vibrational quantum number	$\|\langle c\,^3\Sigma^+ \| C\,^1\Pi \rangle\|$[b]	Percent of maximum overlap[b]
0	8.3×10^{-5}	0.10
1	2.6×10^{-4}	0.36
2	5.8×10^{-4}	0.87
3	1.1×10^{-3}	1.70
4	1.8×10^{-3}	2.92
5	2.6×10^{-3}	4.52
6	3.6×10^{-3}	6.52
7	4.6×10^{-3}	8.82

[a] All values are unitless
[b] See text

caused by the fact that the $^1\Pi$ and $^3\Sigma$ surfaces are *not* intersecting at the energy of the specific state being considered.
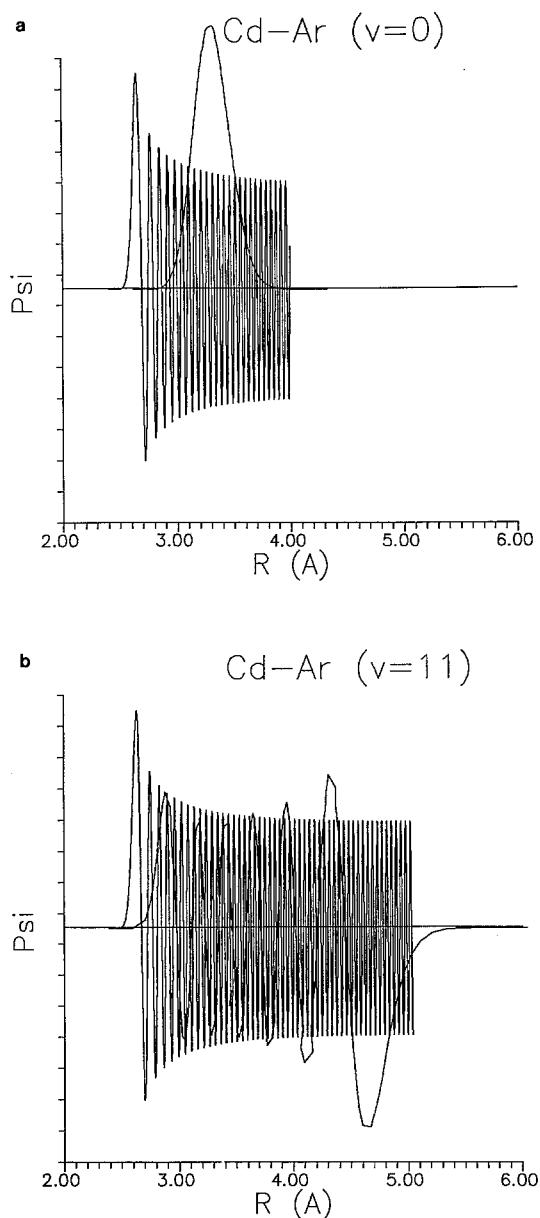
The data in Table 4 show that both the overlap magnitudes and the percentages relative to the "idealized" surface intersection case increase with increasing vibrational quantum number. These data imply that the $C\,^1\Pi$ and $c\,^3\Sigma^+$ curves move closer as the vibrational energy of the $C\,^1\Pi$ state increases and that there is a concomitant increase in the likelihood of a vibronic coupling of these two states.

3.3.4. CdAr. There are twelve observed vibrational levels ($v = 0-11$) for CdAr [6]. Figures 5a and 5b are plots of the $v = 0$ and $v = 11$ vibrational eigenfunctions, respectively, of the $C\,^1\Pi$ state superimposed on the corresponding continuum eigenfunctions of the underlying $c\,^3\Sigma^+$ state. Note that the oscillations of the continuum eigenfunctions are more rapid for CdAr than for MgAr. This is due to the larger $^1P - \,^3P$ energy difference in Cd (1.69 eV) relative to Mg (1.65 eV).

Table 5. Values of nuclear wavefunction overlap integrals of CdAr[a]

Vibrational quantum number	$\|\langle c\,^3\Sigma^+ \| C\,^1\Pi \rangle\|$[b]	Percent of maximum overlap[b]
0	5.9×10^{-7}	0.00
1	4.2×10^{-7}	0.00
2	1.5×10^{-6}	0.00
3	2.3×10^{-6}	0.00
4	3.4×10^{-6}	0.01
5	6.7×10^{-6}	0.01
6	1.1×10^{-5}	0.02
7	1.8×10^{-5}	0.04
8	2.6×10^{-5}	0.06
9	3.6×10^{-5}	0.08
10	1.7×10^{-5}	0.11
11	5.9×10^{-5}	0.15

[a] All values are unitless
[b] See text

a

Cd−Ar (v=0)

Psi

R (A)

2.00   3.00   4.00   5.00   6.00

b

Cd−Ar (v=11)

Psi

2.00   3.00   4.00   5.00   6.00

R (A)

Fig. 5. a Morse potential vibrational eigenfunction of the $v = 0$ vibrational level of $C \, ^1\Pi$ CdAr and the isoenergetic continuum eigenfunction of the underlying $c \, ^3\Sigma^+$ state. **b** Morse potential vibrational eigenfunction for the $v = 11$ vibrational level of $C \, ^1\Pi$ CdAr and the isoenergetic continuum eigenfunction of the underlying $c \, ^3\Sigma^+$ state

As with MgAr, the $v = 0$ plot (Fig. 5a) shows virtually zero overlap of the innermost envelopes of the respective eigenfunctions. However, even for $v = 11$, there is still very little overlap of the inner envelopes (see Fig. 5b). Table 5 summarizes the computed overlaps and the maximum overlap percentages for each of the twelve observed vibrational levels of $C \, ^1\Pi$ CdAr.

As in MgAr, both the overlap magnitudes and percentages increase with increasing vibrational quantum number. However, both sets of data are signifi-cantly smaller than their MgAr counterparts because the $^3\Sigma$ and $^1\Pi$ curves do

not approach as closely for CdAr as for MgAr in the energy range where bound vibrations exist on the $^1\Pi$ state.

These qualitative results indicate (ignoring the difference in magnitude of Cd and Mg spin-orbit couplings) that CdAr is less likely to undergo non-adiabatic coupling of the $C\ ^1\Pi$ and $c\ ^3\Sigma^+$ states than is MgAr.

4. Conclusions

This paper has attempted to provide a detailed look at the ground state and several of the excited state potential curves of the diatomic molecules MgAr, CdAr, and BeAr. Although dispersion contributions to the interaction energies were not included, available experimental data allows us to properly represent minima in even the weakly bound ground states of MgAr and CdAr.

In contrast to implications from experimental studies of CdXe, our computed potentials show *no intersection* of the $C\ ^1\Pi$ and $c\ ^3\Sigma^+$ states in regions below the energetically accessible ^1P Mg (or ^1P Cd) $+\ ^1S$ Ar limit, even when dispersion energies are considered. We conclude that the very deep well (ca. 2500 cm^{-1}) on the $^1\Pi$ surface of CdXe gives rise to an intersection with the $^3\Sigma$ surface, but that analogous intersections cannot occur for CdAr or MgAr because of their much shallower (ca. 544 and 368 cm^{-1}, respectively) $^1\Pi$ state wells.

The above interpretation is in agreement with the observations that $^1\Pi$ excited CdXe produces copious amounts of ^3P_J Cd atoms (presumably via the $^3\Sigma$ surface) and that $^1\Pi$ excited CdAr and MgAr produce little if any ^3P_J Cd or Mg.

The fact that $^1\Pi$ CdAr does not generate ^3P Cd atoms (although the spin-orbit coupling in CdXe is not likely to be greatly different from that in CdAr) suggests that the $^1\Pi$ and $^3\Sigma$ surfaces must intersect for efficient quenching to occur. For CdXe, the surfaces intersect, but for CdAr they do not. However, because the two surfaces in question approach quite closely for CdAr, we decide to explore how a spin-orbit plus non-adiabatic coupling mechanism's rates would vary as a function of splitting between the $^1\Pi$ and $^3\Sigma$ surfaces.

This mechanism, whose strength depends on the overlaps of the bound vibrational eigenstates of the $C\ ^1\Pi$ state and the isoenergetic continuum eigenstates of the underlying $c\ ^3\Sigma^+$ state, was therefore examined in a qualitative manner. Calculation of the overlaps of the nuclear-motion wavefunctions of the $c\ ^3\Sigma^+$ and $C\ ^1\Pi$ states suggest that vibronic coupling is stronger in MgAr than in CdAr. Of course, the spin-orbit coupling is larger for CdAr than for MgAr, so the overall rate, which depends on the *product* of the spin-orbit and non-adiabatic factors, is expected to be small for both MgAr (due to the small spin-orbit factor) and CdAr (due to the small overlap factors).

Finally, the $D\ ^1\Sigma^+$ and $E\ ^3\Sigma^+$ states of BeAr are predicted to be bound by 770 and 900 cm^{-1}, respectively, and thus may constitute interesting synthetic targets for the experimentalist.

References

1. Duval MC, D'Azy OB, Breckenridge WH, Jouvet C, Soep B (1986) J Chem Phys 85:6324
2. (a) Breckenridge WH, Merrow CN (1988) J Chem Phys 88:2329
   (b) Kolwaski A, Funk DJ, Breckenridge WH (1986) Chem Phys Lett 132:263
   (c) Breckenridge WH, Merrow CN (1988) J Chem Phys 88:2320
   (d) Wallace I, Bennett RR, Breckenridge WH (1988) Chem Phys Lett 153:127
3. Bennett RR, McCaffrey JG, Wallace I, Funk DJ, Kowalski A, Breckenridge WH (1989) J Chem Phys 90:2139
4. Bennett RR, McCaffrey JG, Breckenridge WH (1990) J Chem Phys 92:2740
5. Kvaran A, Funk DJ, Kowalski A, Breckenridge WH (1988) J Chem Phys 89:6069
6. Funk DJ, Kvaran A, Breckenridge WH (1989) J Chem Phys 90:2915
7. Funk DJ, Breckenridge WH (1989) J Chem Phys 90:2927
8. Pouilly B, Lengsfield BH, Yarkony DR (1984) J Chem Phys 80:5089
9. Funk DJ, Breckenridge WH, Simons J, Chalasinski G (1989) J Chem Phys 91:1114
10. Hilwa M, Daudey JP (1988) Chem Phys Lett 153:471
11. Okunishi M, Yamanouchi K, Tsughiyo S (1989) Chem Lett 393.
12. Czuchaj E, Sienkiewicz J (1984) J Phys B 17:2251
13. Czuchaj E, Stoll H, Preuss H (1987) J Phys B 20:1487
14. Kaufmann JJ (1973) J Chem Phys 58:4880
15. Stevens WJ, Basch H, Krauss M (1984) J Chem Phys 81:6026
16. McLean AD, Chandler GS (1980) J Chem Phys 72:5639
17. Krishnan R, Binkley JS, Seeger R, Pople JA (1980) J Chem Phys 72:650
18. Hay PJ, Wadt RJ (1985) J Chem Phys 82:270
19. The Utah MESS-KIT is a suite of highly modular codes that were programmed in-house to give a variety of electronic structure functionalities by JA Nichols, MR Hoffman, RA Kendall, HL Taylor, DW O'Neal, E Earl, R Hernandez, M Gutowski, J Boatz, K Bak, J Anchell, X Wang, M Feyereisen, and J Simons
20. Boys SF, Bernardi F (1970) Mol Phys 19:553
21. Morse PM (1929) Phys Rev 34:57